Static and Dynamic Behavior in Model Dendrimer Melts: Toward the Glass Transition

K. Karatasos

Chemical Engineering Department, Chemistry Section, Physical Chemistry Lab, University of Thessaloniki, 51114 Thessaloniki, Greece

Received January 25, 2005; Revised Manuscript Received March 21, 2005

ABSTRACT: Molecular dynamics (MD) simulations were employed in order to explore the static and dynamic response of model AB2 dendrimer melts of generations 3 and 4, in a temperature range covering the states of enhanced mobility, as well as the states where a significant dynamic slowdown led to a virtual freezing-in of the dendrimer motion. Particular emphasis was given to the investigation of the motional and conformational changes of the models in the proximity of a glasslike transition observed upon temperature decrease. The qualitative picture emerging from this study is consistent with recent pertinent experiments, offering thus the possibility for a better understanding of basic mechanisms responsible for the observed behavior.

I. Introduction

Polymers bearing the dendritic topology have emerged as important materials for a large number of novel nanoscale applications.[1−4] Their intermediate nature between linear polymers and colloids[5−8] renders them as ideal candidates when combination of properties of these two classes of materials is desired. This perspective is strongly promoted by the recently developed chemistry protocols, which allow a molecular-level engineering of their topological and other physical (mechanic, thermodynamic, electric, etc.) characteristics.[9−11] Furthermore, the control of chemistry has enabled the synthesis of dendrimers with such a level of uniformity in their structure that can be closely compared to models often employed in theoretical and computational studies, offering thus a solid ground for a closer comparison between experiment and theory.

Such a comparison concerning the behavior of dendrimer molecules in the solution state has significantly been advanced in recent years[12−18] to a point where theory can actually act as a guide for new experiments and targeted synthesis.[5] On the other hand, there is a relatively limited progress regarding an analogous comparison of the behavior of dendritic molecules in the melt, despite the constantly increasing number of modern applications associated with use of dendrimers in the absence of solvent.[19−25] Although several experimental investigations have been carried out shedding light on different aspects of dynamic, thermodynamic, and rheological behavior of dendrimer melts,[26−33] only few theoretical and computational efforts have addressed similar issues.[34−37]

Among the central subjects intimately related to important physical properties of these materials in the bulk[31] is the temperature dependence of their structural/conformational and dynamic features, particularly close to the characteristic temperature where a glasslike transition associated with a "freezing-in" of motional degrees of freedom takes place.[29,34−37] The significance of glass-transition-related phenomena in the behavior of polymeric[38−40] and colloidal[41−44] systems cannot be overemphasized, as it has been—and continues to be—a subject of intense scientific effort over the years. Considering that a combination of polymer/colloidal features is manifested in dendrimer behavior (and even more so in a "tunable" manner), elucidation of the mechanisms leading to vitrification of these materials appears as a challenging task.

It is the aim of the present work to contribute toward this direction, by examining changes in the static and dynamic behavior of model dendrimer melts, upon cooling from elevated temperatures to the vicinity where a significant dynamic slowdown of dendrimer motion occurs.

II. Description of the Models

As the scope of this effort is to explore generic behavior owing to the dendritic topology while keeping compatibility with earlier work[18] for comparison purposes, a united atom (UA) representation of each dendrimer bead was adopted bearing mass corresponding to a CH_i group, where i is determined by the connectivity of each bead. The dendritic topology employed for each individual dendrimer molecule is schematically presented in Figure 1. The concentric circles denote the boundaries of the two innermost generational shells.

The number of beads up to the g_{th} generational shell is given by the general formula

$$N(g) = 1 + fP\frac{(f-1)^{g+1}-1}{f-2} \tag{1}$$

where f is the functionality of the branching points and P is the number of bonds (spacers) between branching points. In the models adopted, the structure emanates from a trifunctional core ($f = 3$) and proceeds radially outward with branching points at every other bead ($P = 2$). The generational index (starting from $g = 0$) of the outermost shell for a given dendrimer model will be denoted by G, to which we will henceforth refer to as the generation of the dendrimer.

For the bulk state representation, dendrimer models consisting of 30 molecules each were prepared as described in section III, and molecular dynamics trajectories were generated at a broad temperature range covering both enhanced and reduced mobility regimes. To check possible dependence on dendrimer generation

10.1021/ma050155x CCC: $30.25
Published on Web 04/13/2005

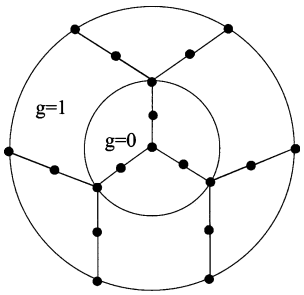

Figure 1. Schematic representation of the dendrimer models.

(and consequently on systems' size), simulations of models of two different generations, namely G3 and G4, were performed.

III. Simulation Details

Throughout the simulation stages as will be described below, inter- and intramolecular interactions were accounted for by means of the DREIDING force field[45] which has successfully been employed in the past for simulations of dendrimer systems.[35,46−48] For comparison purposes to past investigations where the same force field was utilized, as well as for computer time saving, no extra terms involving many-body interactions were considered. According to this force field, the potential energy function bears contributions from bond stretching, angle bending, and dihedral angle rotation. Stretching of bonds between atoms of types i, j is described by a harmonic form $^1/_2 k_{b_{ij}}(b_{ij} - b_{ij}^0)^2$, where $b_{ij}^0 = b_i^0 + b_j^0 - \delta$ with $\delta = 0.01$ Å and $k_{b_{ij}} = 700$ kcal/(mol Å^2). For all UA $b_i^0 = 0.770$ Å was used, resulting to $b_{ij}^0 = 1.53$ Å. Angle bending is described by a harmonic cosine form $^1/_2 k_\theta(\cos\theta - \cos\theta^0)^2$ for all kinds of angles, with $k_\theta = 100/(\sin\theta^0)^2$ kcal/mol and $\theta^0 = 109.471°$. Torsional angle rotation is accounted for by a contribution of the form $^1/_2 k_\phi\{1 - \cos[n(\phi - \phi^0)]\}$, where $k_\phi = 2.0$ kcal/mol (overall), $n = 3$, and $\phi^0 = 180°$. A Lennard-Jones potential $\epsilon_{ij}[(\sigma_{ij}/r_{ij})^{12} - 2(\sigma_{ij}/r_{ij})^6]$ is employed for the calculation of nonbonded interactions between any ij pair of united atoms separated by a distance r_{ij} with a cutoff of $r_{cut} = 10$ Å. Parameters ϵ_{ij} and σ_{ij} are derived from combinations of the parameters corresponding to the individual CH_i and CH_j UA types according to $\epsilon_{ij} = (\epsilon_i\epsilon_j)^{1/2}$ and $\sigma_{ij} = (\sigma_i + \sigma_j)/2$. Individual parameters ϵ_i, σ_i for UA with $i = 1, 2, 3$ implicit hydrogens are 0.1467, 0.1984, 0.2500 kcal/mol and 3.9830, 4.0677, 4.1524 Å, respectively.

Initial single-dendrimer models of generations G3 and G4 were generated following the procedure described in ref 49. Melt systems comprised by 30 dendrimer molecules for each generation were constructed by the aid of the Amorphous cell module (Molecular Simulations Inc., now Accelrys Inc.) at an elevated temperature ($T > 750$ K). Subsequently, each melt was subjected to MD cooling under constant pressure ($p = 1$ atm) and temperature conditions in steps of 50 K, down to 300 K. Further cooling of the systems was realized by steps of 20 K down to 280 K for G4 and 260 K for G3 systems, respectively.

During the cooling process, each system spent typically about 100 ps (in 1 fs steps) at each temperature (except at $T < 300$ K where the systems stayed longer), followed by about 40 000 steps of steepest descent and conjugate gradient energy minimization cycles. To allow for further relaxation of the model configurations,

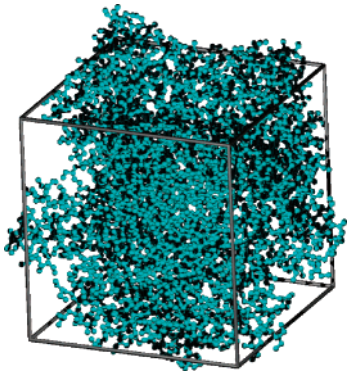

Figure 2. Equilibrated G4 model at 550 K.

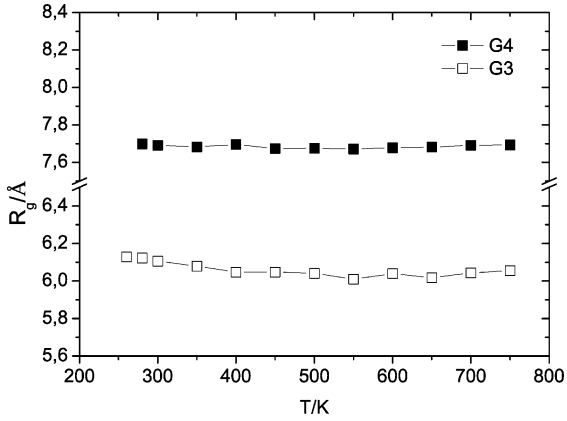

Figure 3. Temperature dependence of the radius of gyration. The error bars are comparable to the symbols' size.

isobaric−isothermal (NPT) MD equilibration ($p = 1$ atm) of 1−2 ns periods were performed until certain energetic (stabilized potential and total energy with small relative energy fluctuations), thermodynamic (stable average of the specific volume), and conformational (stable average of radius of gyration) criteria were met. Figure 2 depicts an equilibrated model at $T = 550$ K for the G4 system.

Ensuing to the equilibration time, trajectories in the NPT ensemble (employing periodic boundary conditions in cubic box and using the Nosé−Hoover thermostat[50] and a barostat based on the Hoover algorithm[51]) of several nanoseconds length (10−24 ns depending on the temperature and the size of the models) at $p = 1$ atm, with a time step of 1 fs, were produced by a suitably modified version of the DLPOLY molecular dynamics program.[52] The data analysis routines were developed by the author. At all temperatures examined, the standard deviation related to temperature fluctuations ranged between 4 K ($T < 350$ K) and 10 K ($T > 650$ K).

IV. Static/Structural Characteristics

A. General Features. Figure 3 shows the variation of the radius of gyration (R_g) of the examined models with temperature. For both generation systems, their characteristic size appears to be insensitive to temperature at the temperature range examined. The minor variation of R_g at the G3 model amounts to less than 2% of the average, while for the G4 model it is virtually temperature independent. Compared to analogous freely jointed models at solution close to Θ conditions,[18] dimensions of the melt systems are reduced by about 16% on average. This difference can be accounted for by the angle bending and torsional terms introduced to the potential energy expression of the current models, which render them more compact.

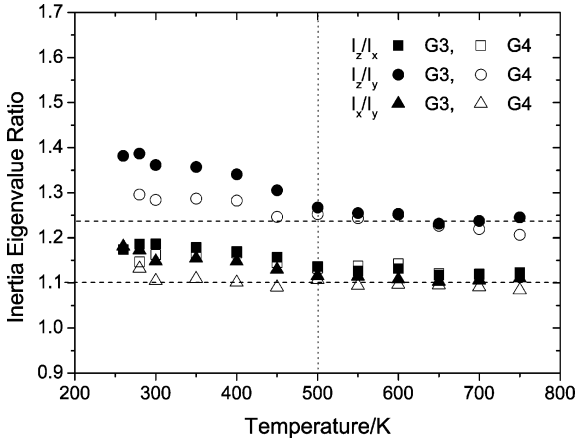

Figure 4. Aspect ratios of the principal moments of inertia as a function of temperature. Error margins are comparable to symbols' size. Dashed lines denote the high-temperature behavior of the aspect ratios, while the vertical dotted line marks the location of the onset of deviation from this behavior.

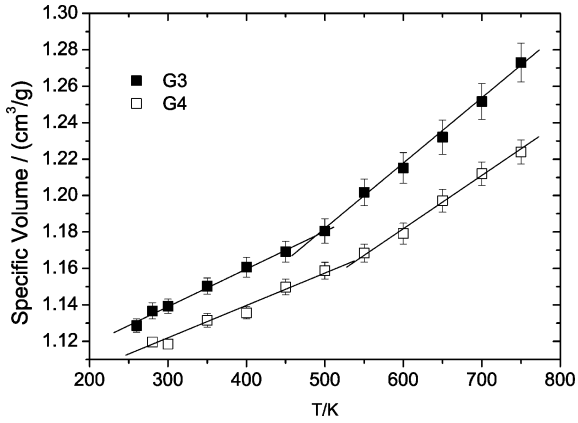

Figure 5. Temperature dependence of the specific volume.

To examine the effect of temperature on other geometrical attributes like the symmetry of the dendrimers' shape, we have calculated the eigenvalues of the moment of inertia tensor and their relative ratios I_z/I_x (■, G3; □, G4), I_z/I_y (●, G3; ○, G4), and I_x/I_y (▲, G3; △, G4), as illustrated in Figure 4.

In accordance with previous observations,[18,53,54] aspect ratios retain values above but close to unity for these relatively low generation dendrimers, with the G4 system assuming a lower degree of asymmetry in its shape. The most interesting feature, though, arises from the temperature dependence of the respective ratios: below approximately 500 K a deviation from the higher temperature behavior is observed (more prominent in the G3 model), signifying a passage from a more symmetrical globular shape to that of a more elongated spheroid geometry. Such a morphological "transition" might be related to a different local packing realized at lower temperatures, which in turn could be associated with density changes. The temperature dependence of the specific volume of the examined systems is presented in Figure 5.

For both generation dendrimers, an apparent change of slope is noted at temperatures close to 500 K. Monitoring the temperature dependence of the specific volume is a method commonly utilized in experimental[55] and simulational[56] studies in order to locate the phenomenological glass transition (T_g) in polymeric systems. In this context, the observed behavior strongly

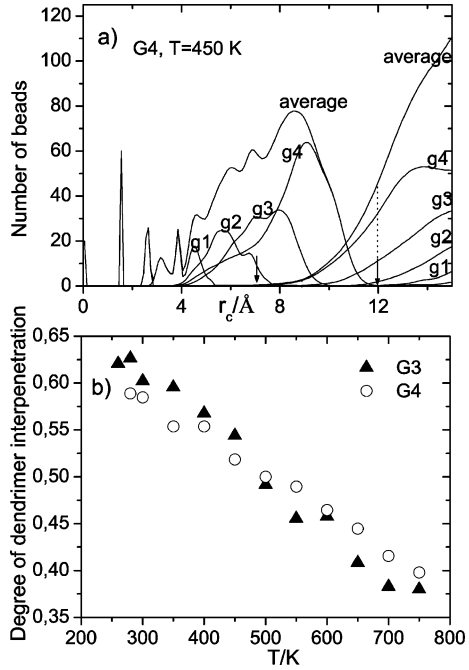

Figure 6. (a) Overlap between intra- and intermolecular distributions of dendrimer beads with respect to the distance from the core bead (r_c) for the G4 model at 450 K. Arrows indicate the integration limits (see text). (b) Temperature dependence of the degree of interpenetration for both generation models.

indicates that a similar transition occurs in the dendritic models. The moderately higher temperature at which the break of the slope in G4 model occurs is consistent with relevant experimental results[29,37] and theoretical approaches for the dendrimer glass transition.[36]

B. Morphological Details. *1. Average Dendrimer Interpenetration.* The occurrence of morphological changes, as detected earlier at nearby temperatures, alludes to a direct correlation with this phenomenological glasslike transition, emphasizing the synergy of intramolecular and intermolecular effects to the manifestation of glass phenomena in dendrimer systems. One of these effects was conjectured[8] to be the degree of interpenetration between different dendrimer molecules, which might play an important role much in analogy to the behavior of "soft" colloidal systems or star molecules possessing low or high functionalities. Along these lines we have examined the degree of interpenetration between dendrimer molecules as a function of temperature for both generation models. The procedure followed for this calculation is schematically presented at one temperature in Figure 6a for the G4 model. Taking the central bead of each molecule as reference, we have constructed the distribution of the beads at distances (r_c) extending up to approximately twice the radius of gyration. Contributions from beads belonging to the same dendrimer were separated from those belonging to different molecules, while at the same time contributions from distinct generational shells were resolved as well. The leftmost distribution in Figure 6a involves beads comprising a single dendrimer ("intra"), while the rightmost curves describe distributions of beads belonging to different molecules ("inter"). Distributions denoted as "average" result from the summation of the contributions of all corresponding generational shells. Visual inspection of the leftmost distribution confirms once more the experimental finding[57−59] of the backfolding of beads belonging to the outer generational

shells toward the topological center. Comparing the shapes of the distributions of different generational shells to the respective ones describing the analogous freely jointed models,[18] it becomes apparent that the former are less broad, with the peaks shifted toward the dendrimer's periphery. The "degree of interpenetration" is calculated by the area under the average "inter" curve (between limits defined by the points where the two average distributions become zero) divided by the total number of beads per dendrimer.

Following this procedure for all temperatures, Figure 6b is constructed. The main feature emerging from this picture is that for both generations the degree of interpenetration increases apparently in a linear fashion upon temperature decrease. Augmentation of the interpenetration degree on temperature decrease is not unexpected in view of the corresponding increase in density, but this being realized in a seemingly constant rate is not straightforward. One more point that must be noticed is that the two virtual lines that could describe the temperature dependencies seem to cross at some temperature, with the one corresponding to the smaller size model (G3) being steeper. In a previous simulational study[35] of dendrimer melts of different generation models but at a fixed temperature (400 K), it was found that interpenetration of individual molecules decreased upon increase of the dendrimer size. This observation was ascribed to the increase of compactness of the structure as the generation becomes higher. According to the previous discussion, the same behavior seems to hold for our models (at least for the two generations studied here), but only at sufficiently low temperatures (here, below the crossing of the two virtual lines). On these grounds, aside from the specific dendrimer topology, one may have to take into account one more parameter, temperature, if the argument relating dendrimer size with compactness is to be generalized.

2. Static Structure and Local Packing Characteristics. For more detailed information concerning local packing and related structural changes incurred by temperature decrease, analysis methods affording higher spatial resolution are required. Along these lines, to elucidate characteristics of the dendrimers' arrangement in different spatial scales, we have calculated radial distribution functions (rdf) (see ref 60) as well as static structure factors, separating intramolecular from intermolecular contributions.

For isotropic media, the static structure factor can be computed by[60]

$$S(q) = 1 + \frac{N}{V}\int [g(r) - 1]\frac{\sin(qr)}{qr}\, 4\pi r^2\, \mathrm{d}r \qquad (2)$$

where q is the magnitude of the scattering vector, N is the total number of scatterers (beads) inside the volume of the system, V is the average volume, and $g(r)$ denotes the radial distribution function (r is the distance between any two beads). If scattering arising solely from beads belonging to a single dendrimer molecule is taken into account, the so-called form factor of the molecule can be calculated.[61]

$$F(q) = 1 + \frac{1}{N}\left\langle \sum_{j=1}^{N}\sum_{j\neq i}^{N} \frac{\sin(qr_{ij})}{qr_{ij}} \right\rangle \qquad (3)$$

N is the number of beads per molecule, and r_{ij} the distance between beads i and j, while the angular brackets denote time and ensemble average. When invoking eqs 2 and 3, all UA beads are treated in an equivalent manner.

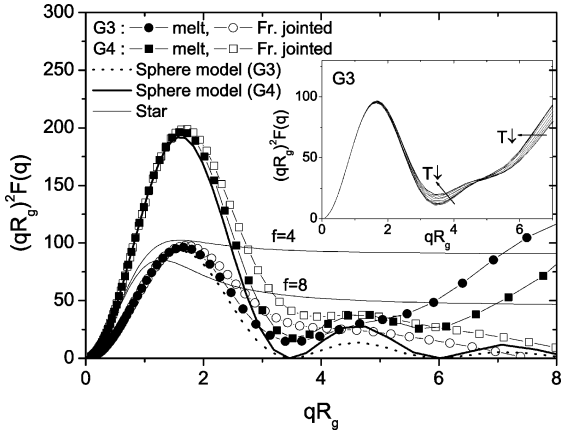

Figure 7. Collation of the form factors between melt (T = 450 K) and freely jointed solution models of G3 and G4 dendrimers in the Kratky representation. Star polymer (number of arms $f = 4$ and $f = 8$ with Gaussian statistics) and homogeneous sphere, with radii equal to the R_g of the G3 dendrimer model form factors, are shown for comparison. Inset: temperature dependence of the form factor for G3 melt model. Arrows point to the direction of temperature decrease.

Form factor provides information pertinent to the geometry of a single molecule in its respective environment and is usually employed as a sensitive tool for the identification of subtle topological differences among similar molecular structures.[5,17] Such structural differences between freely jointed dendrimer systems in solution[18] and the corresponding melt models studied in the present work are illustrated in Figure 7. At the same figure, theoretical curves representing homogeneous spheres and multiarm star models are included for comparison. Location of the first peak at $qR_g \simeq 1.7$ and a clear indication for secondary maximum at $qR_g \simeq 4-5$ are common features between solution and melt systems. For both sets of models, the secondary maximum is more prominent at the higher (G4) generation, in line with previous results[17,62,63] where it was found that the higher the generation, the closer the dendrimer geometry to a homogeneous globular shape. At $qR_g > 5$, however, the behavior of the melt models appears to be consistent with that of a spherical shape with fuzzy shell and internal density fluctuations.[17] The temperature dependence of the form factor of the melt models (shown as inset for the G3 systems) implies a modification of geometry in consensus with the findings from the inertia tensor eigenvalues (Figure 4).

Assessment of the relative role of intramolecular and intermolecular effects on dendrimer melt morphological characteristics can be carried out in more detail by examining radial distribution functions and the related static structure factors. Figure 8 presents dendrimer density/bead distributions and radial distribution functions for the systems studied. Panels (a) of Figure 8 depict the average number density profile $\rho(r_c)$ (left axis) and the corresponding bead distribution $b(r_c)$ (right axis) at T = 500 K as a function of the distance from the central bead r_c. The number density profiles resolved to contributions from different generational shells are presented in the insets. The sharp peaks at low r_c arise from characteristic distances or local conformations inherent to the model, like the length of a single bond, that of beads forming a bending angle, a dihedral angle,

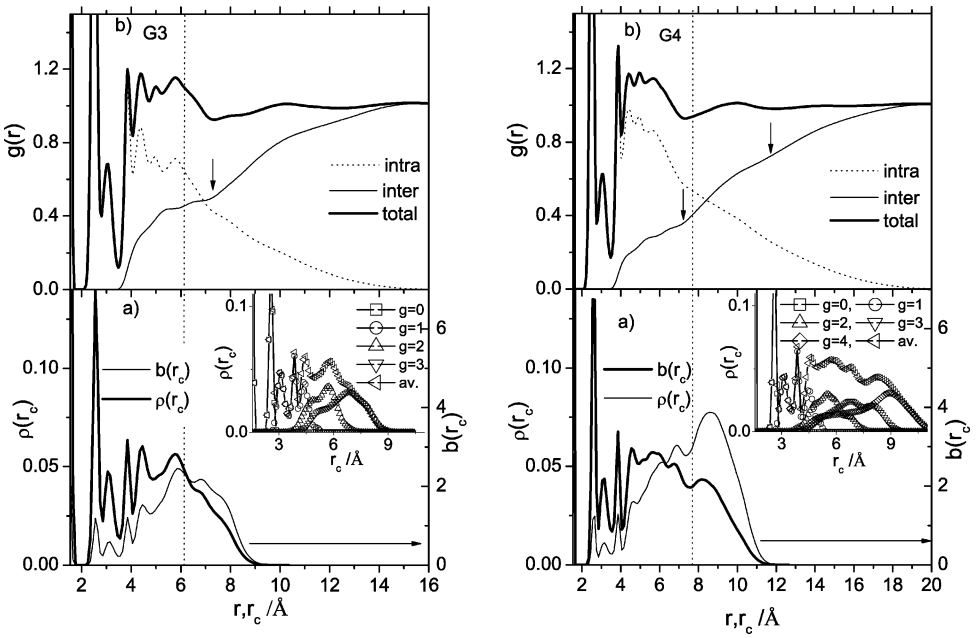

Figure 8. (a) Average number density $\rho(r_c)$ (left axis) and bead distribution $b(r_c)$ (right axis). Insets show density profiles resolved in generational shells. (b) Total intra- and intermolecular radial distribution functions. Vertical dotted lines denote the positions of the corresponding R_gs. Arrows mark inflection points of the intermolecular radial distribution functions.

etc. At distances longer than the respective R_gs, average density profiles exhibit a monotonic decrease toward zero. At shorter distances, only at the larger model's distribution, does a region (4 Å$< r < R_g$) of slowly varying density bear resemblance to the one observed in the analogous freely jointed solution models.[18] These variations of the density profiles are essentially reflected to the intramolecular contributions in the behavior of the radial distribution function as demonstrated in panels (b). It is of interest to note that intermolecular contributions become significant at distances well below the corresponding radii of gyration (marked by the vertical dotted line), signifying that local density within a dendrimer molecule in the melt can be significantly affected by the presence of beads from the neighboring molecules. Actually, as follows by the variation pattern of the intermolecular contribution, distinct probability regions (demarcated by the inflection points) for the presence of beads belonging to neighboring molecules can be formed.

To afford better spatial resolution while providing data which are more convenient in terms of comparison to experiment, the static structure factor of the models was calculated (eq 2) and compared to that of a linear polymer analogue,[64] as illustrated in Figure 9.

At scattering vector magnitudes $q > 1$ Å^{-1} the static structure factors of the dendrimers essentially follow the modulation of that of the linear polymer. It worths noticing that dendrimer models exhibit a strong peak (peak 3 in inset) at practically the same location as the intermolecular peak of the linear chains, which is related to a length scale pertinent to local cooperative rearrangements which contribute to α-relaxation and hence glass transition phenomena.[65] However, whether it is sound to draw analogies regarding the intermolecular nature of this peak in dendrimers and its role in glass transition remains to be determined, particularly in view of the existence of extra peaks—not present in linear polymers—at lower values of the scattering vector. A magnification of the low-q window is shown in the inset of Figure 9. Apparently, characteristics of

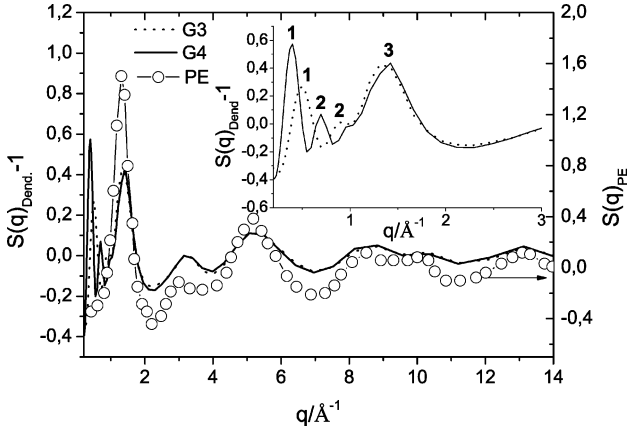

Figure 9. Comparison of the static structure factor describing a linear polyethylene (PE) chain at 430 K and the two different dendrimer models at 450 K. Inset: magnification of the low-q regime. The peaks are labeled for reference purposes.

the additional peaks are dendrimer size dependent. The corresponding length scales are comparable, or even exceed those of the respective radii of gyration, implying interdendrimer correlations. The length scale associated with the lowest-q maximum (peak 1) is of the order of twice the respective R_gs, while that of the next maximum (peak 2) appears somewhat larger (15−20%) than the corresponding radii of gyration.

To further elaborate on the origin of the observed peaks, we have separated inter from intra contributions to the structure factor, as shown in Figure 10. In this figure the total static structure factor together with the distinct contributions arising from the inter part of $g(r)$ via eq 2 (labeled as inter), and the form factor calculated directly in the inverse space according to eq 3 (labeled as intra) are plotted. Comparing features between the total and the partial structure factors, it appears that the larger contribution responsible for peak 2 of the total $S(q)$ is of intermolecular origin, while for peak 3 apparently both intramolecular and intermolecular contributions are combined. Since the length scale ($2\pi/q$) asso-

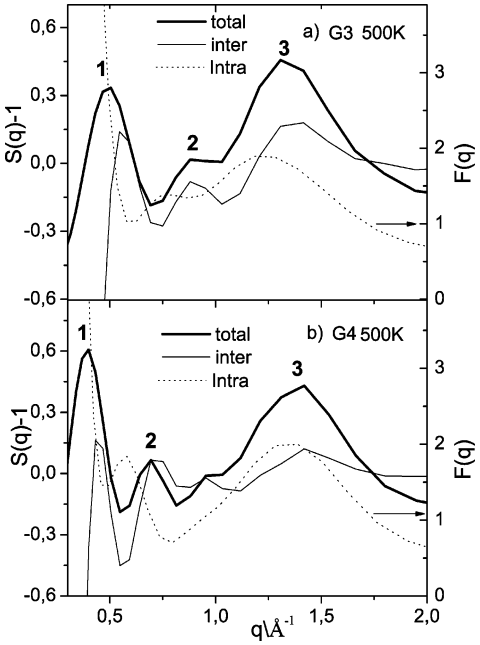

Figure 10. Separation of intramolecular (intra) and intermolecular (inter) contributions to the total structure factor: (a) G3 model; (b) G4 model. The index assigned to each peak is the same as in the inset of Figure 9.

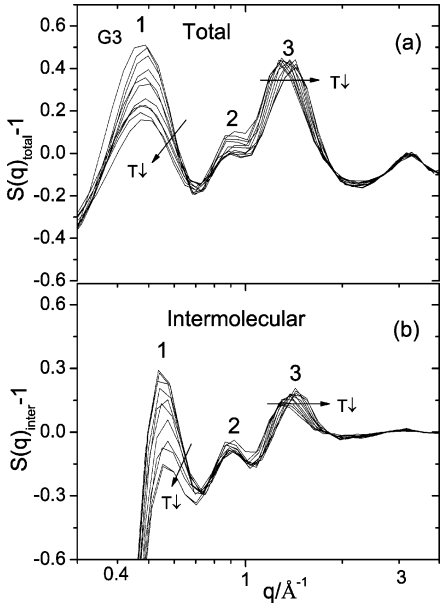

Figure 11. Temperature dependence (260−750 K) of the static structure factor for the G3 model: (a) total; (b) inter. Arrows point to the direction of temperature decrease.

ciated with peak 3 is shorter than the corresponding R_g, it can be surmised that this maximum is due to the presence of beads of neighboring dendrimers involved in a rather deep ("inner") interpenetration, together with beads belonging to the two outermost generational shells of the dendrimer. Peak 2 corresponds to a separation distance larger than R_g but still within the limits of the dendrimer periphery, suggesting the existence of a more superficial ("outer") interpenetration shell. This picture is consistent with the one described earlier, when features of the intermolecular rdf were discussed. Peak 1 refers to separation distances comparable to twice the respective R_gs, implying that a preferable interdendrimer packing arrangement characterized by such a distance could be involved. On the other hand, according to the intra part of the rdf and the intradendrimer density profiles shown in Figure 8, intra contributions could also be considered.

The next step is to monitor the changes of the spectral characteristics of $S(q)$ as a function of temperature. Figure 11 portrays the temperature dependence of the total and the intermolecular part of the static structure factor for the G3 models. Behavior of G4 models (not shown here) exhibits similar features.

Monitoring total $S(q)$ (Figure 11a) becomes clear that peaks describing different length scales respond to temperature changes in a distinct manner. The sole effect on low-q maxima (peaks 1 and 2) appears to be an intensity reduction on temperature decrease, which to a large extent can be accounted for by a similar decrease observed in their intermolecular analogues. This amplitude reduction occurring in the lower-q peaks indicates a corresponding loss of coherence of the microstructure at length scales close to, or larger than, the dendrimer size. Regarding peak 3, the moderate intensity rise at lower temperatures exhibited by the intermolecular part should be compensated by an analogous decrease of the intramolecular contribution, since no amplitude attenuation is observed in the total structure factor. The most intriguing characteristic of the high-q maximum present in both the intermolecular and the total structure factor is the shift of the peak position to higher q values upon cooling.[66] As was discussed earlier, this peak appears essentially at the same q value as the intermolecular diffraction peak of a linear polymer, whose location is also known to be temperature dependent.[65] In linear polymers this effect reflects the modification of local packing with temperature, which eventually leads to glass transition phenomena at lower temperatures. In the case of dendrimer melts, changes of the local packing involving interdendrimer motion can be realized through the mechanism of interpenetration which increases as temperature lowers. In the context described earlier regarding the origin of peak 3, the shift in its position can be viewed as a consequence of increased interpenetration, which would bring the pertinent scattering centers closer and thus shift the diffraction peak to higher scattering vector values. Moreover, this scenario would provide a direct link between this diffraction peak and a mechanism that is related to dendrimer glass transition.

To collect more information regarding the interdendrimer arrangement, we can examine whether any kind of long-range order is present (or is induced due to temperature changes) in these systems. To this end, one can treat every dendrimer molecule as a single "scatterer" represented by its center of mass (CM) location and use an expression like eq 3 in order to calculate the corresponding static scattering function directly in the inverse space. The results of this calculation are shown in Figure 12.

It is apparent that these systems exhibit a liquidlike ordering, which can be considered as an "amorphous" state for polymeric materials.[56] The relative locations of the observed peaks corroborate this notion.[67] This kind of liquidlike ordering has also been observed in bulk multiarm star systems in both experiment and simulations,[8,68,69] while it has recently been noticed in simulations of bead−thread dendrimers models[70] as well. The location of the first peak of the CM structure factors for both generations corresponds to a first-neighbor distance ($2\pi/q_{peak}$) very close to $2R_g$ of the

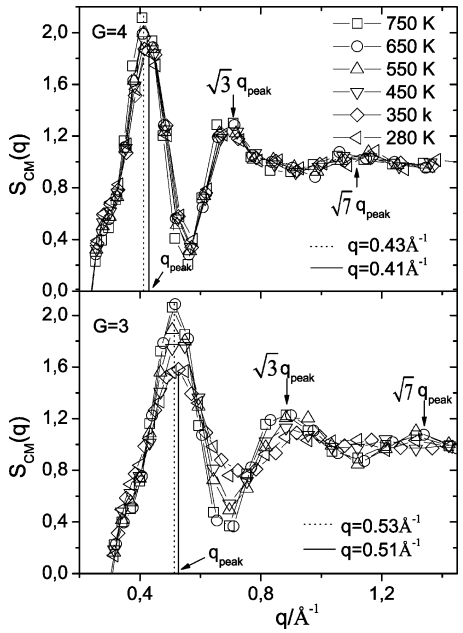

Figure 12. Static structure factors associated with the centers of mass (see text) at temperatures spanning the entire regime examined. Vertical lines mark the locations of the first peak at the two temperature extremes considered. The arrows point to the relative locations consistent to a liquidlike structure.

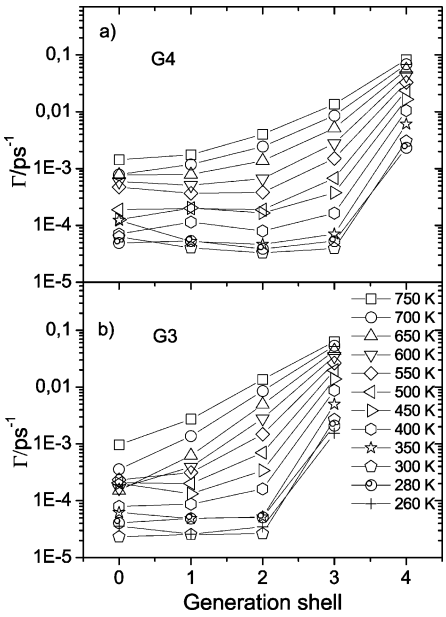

Figure 13. Conformational transition rates as a function of temperature, resolved in contributions from different generational shells for the examined models: (a) G4; (b) G3. Error bars are within the symbols' size.

corresponding dendrimer model. Concerning temperature effects on this picture, it seems that the peaks are slightly shifted upon cooling to higher q values (i.e., dendrimers are getting closer) followed by a minor decrease in their corresponding amplitude; that is, the coherence of the interdendrimer arrangement is slightly decreased, particularly for the lower generation dendrimers.

V. Dynamic Properties

The characteristic signature for the onset of vitrification phenomena in structural glass-forming systems is a dramatic slowdown in the so-called α-relaxation process associated with dynamics at the local scale, involving e.g. rearrangements of several glass-formers in the case of glass-forming liquids or several monomers in the case of polymers. Such a relaxational process has been experimentally detected in dendrimer melts and was demonstrated that the "dynamically" determined glass transition temperature was in a good agreement with the calorimetrically measured one.[32,28]

A. Transition Rates. Among the main motional mechanisms involved in modification of local configurations in dendrimers is the torsional jumps between neighboring trans−gauche conformational states.[71,72] Since local dynamics in dendrimers of a given size depend on the relative position of the relaxing segments with respect to the topological center,[18,46,71,73,74] it is of interest to examine how local mobility due to conformational transitions depends both on temperature and on the relative location of the dihedral angles within the dendrimer structure. Here a transition is counted when a torsional angle rotates from the vicinity of the minima of one of the torsional angle potential energy wells to the minimum of a neighboring well. Transition rates are expressed as number of jumps per dihedral per picosecond. A transition rate map for the examined systems spanning the entire temperature range studied is presented in Figure 13. As a general remark, with the exception of the lower temperatures, transition rates (Γ) increase as a function of temperature and generational shell, as expected. Comparison of same temperature curves between G3 and G4 models at generational shells equidistant from the outer shell reveals that they are almost superimposable, indicating a rather weak dependence on model size. A similar weak dependence on dendrimer size of the average relaxation times describing bond reorientation has been observed in the lower generation (G3, G4, G5) freely jointed analogues.[18] It is of particular interest to note that even at the lower temperatures, dihedrals belonging to the outer shell remain considerably active, in contrast to the behavior even of the adjacent shell. Actually, dihedrals of the adjacent-to-the-outer shell ($g = 2$ and $g = 3$ for the G3 and the G4 models, respectively) exhibit the highest relative decrease in transition rate compared to all others. The high degree of mobility retained at the outer generational shell at temperatures lower than the nominal T_g, provides further insight into recent experimental findings in dendrimer melt systems,[29] where it was observed that crossing the glass transition does not entirely erase the memory of intramolecular mobility, allowing thus survival of sub-T_g motional processes.

Adding up the contributions of all generational shells, the temperature dependence of the *average* transition rates for each model can be mapped out, as illustrated in Figure 14. Average rates follow an Arrhenius dependence with an apparent change of slope at around 500 K. Association of this observation with the modification of structural/geometric characteristics and the change in the specific volume behavior occurred at the same temperature vicinity is straightforward.

B. Dynamic Structure Factor. Examination of "internal" dendrimer dynamics affording spatial resolution within the dendrimer structure can be performed through the calculation of the dynamic structure factor. To capture characteristics of the dynamic response relevant to the overall dendritic structure, we have calculated the coherent dynamic structure factor arising from the collective motion of all beads belonging to a

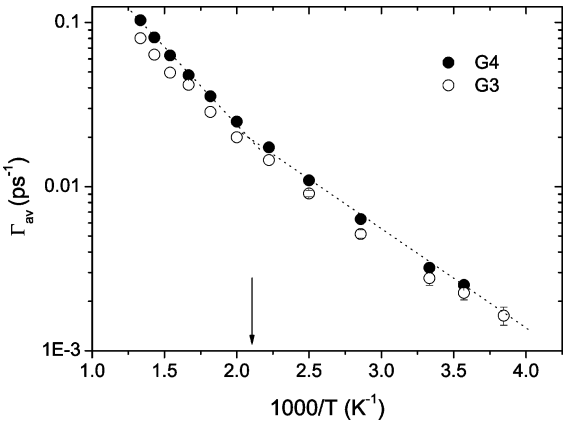

Figure 14. Temperature dependence of the average transition rates (Γ). Lines are guides to the eye. Arrow marks approximately the abscissa corresponding to the change in slope. Nonshown error bars are within the symbols' size.

single dendrimer molecule. The coherent dynamic structure factor for isotropic media normalized by its static behavior is given by

$$\tilde{S}(q,t) = \frac{S(q,t)}{S(q,0)} = \frac{\left\langle \sum_{ij} \frac{\sin[qr_{ij}(t)]}{qr_{ij}(t)} \right\rangle}{\left\langle \sum_{ij} \frac{\sin[qr_{ij}(0)]}{qr_{ij}(0)} \right\rangle} \quad (4)$$

where angular brackets denote ensemble and time average (over all time origins). Indices i,j refer to beads belonging to the same dendrimer while $r_{ij}(t)$ denotes their distance at time t. The calculation was performed in unfolded coordinates. A range of scattering vector magnitudes spanning length scales from that of a single bond up to the overall dendrimer size ($\simeq R_g$) were covered.

Dendrimer dynamic spectra are known to be of complex nature, usually requiring a description that cannot be based merely on consideration of processes well separated in time scale, but instead on a distribution of them associated with a spectrum of relaxation times.[18,73,75] On this basis, analysis was performed via calculation of the distribution of relaxation times (DRT)[76] corresponding to elementary single-exponential processes according to the expression

$$C(t) = \int_{-\infty}^{+\infty} g(\ln \tau) e^{-t/\tau} \, d \ln \tau \quad (5)$$

where $g(\ln \tau)$ symbolizes the normalized (in the logarithmic scale) DRT.[76] In this context, dynamic functions are described without any a-priori assumption regarding the functional form of either the spectra themselves or their corresponding distribution functions $g(\ln \tau)$. Information associated with the existence of distinct motional processes and the dispersion of exponential decays describing each process is extracted from the number and width of the peaks appearing in the DRTs, respectively. A characteristic time (CT) for the i_{th} process appearing in the spectra can be calculated as $\tau_i = \int_{\Delta\tau_i} \tau g(\ln \tau) \, d \ln \tau / \int_{\Delta\tau_i} g(\ln \tau) \, d \ln \tau$, where $\Delta\tau_i$ denotes the time interval over which the i_{th} peak extends. In the case of symmetric peaks, the location of the maximum provides a good estimate of the CT. If the integration is performed over the entire time window, an average time (including the contribution of all the dynamic processes) τ_{av} is calculated.

An example of calculated $\tilde{S}(q,t)$ spectra together with the corresponding DRTs, for various temperatures and constant q value (representing the maximum position of peak 3 of the static structure factor), is plotted in Figure 15 for G3 and G4 models. Lines through the points (upper panels) correspond to the respective fits resulted from the analysis procedure described above. Focusing on the behavior of the DRTs of the G3 model, it becomes obvious that while at high temperatures only a single but broad peak characterizes the spectra, at lower temperatures it is separated to peaks displaying distinct spectral features. The fast ones appear to lose amplitude, while their time scale (approximately defined by their peak location) remains insensitive to temperature change. In contrast, slower processes gain in amplitude and exhibit a strongly temperature-dependent characteristic time. Dynamic processes with spectral features similar to those of the fast process are commonly encountered in polymer dynamics[77,78] and can be ascribed to fast librational motions around the torsional energy minima. On the other hand, the strong response to temperature change of the characteristic time and amplitude shown by the slower process provides a direct link to the dynamic freezing-in of intradendrimer relaxational motions expected in the vicinity of the glass transition.

Examination of the larger (G4) model's DRTs reveals that they share common characteristics with their G3 analogues, like the presence of very fast and ultraslow processes with distinct time and amplitude temperature dependence. Additional features are manifested via the appearance of processes at intermediate time scales even at the highest temperatures examined. Similar intermediate relaxational processes were observed[18] in solutions of the freely jointed analogues of the studied systems but at higher size models. Given that at melt systems higher local densities can be realized at lower generations compared to the solution case, one can follow analogous arguments in order to interpret the observed behavior in terms of a "dynamic layering", according to which areas of distinctly different mobility are formed within the dendritic structure as this grows. Actually, this scenario would be consistent with the existence of multiple glass transitions, should the mobility contrast between the "layers" be sufficiently high so that freezing-in of local motions would occur at different temperatures. Experimental indications of such a behavior in dendrimer melts are already available.[29]

Information regarding the mechanisms responsible for propagation of intradendrimer motion at different length scales can be provided by the q dependence of the characteristic time of the dynamic structure factor. To facilitate comparison to existing or future scattering data on local dendrimer motion, where dynamics arising from distinct processes is rather difficult to be resolved, we have calculated the average relaxation time τ_{av} instead, at different q values and temperatures as outlined in Figure 16. Lines denote the apparent slopes describing q dependence of the average times at the lower and the higher temperatures for which analysis was performed. For both models, a gradual change of slope from -3 to -2 is observed upon temperature decrease. Focusing attention on the low-temperature regime, it appears tempting to associate the q^{-2} dependence with a diffusional dynamic behavior. However,

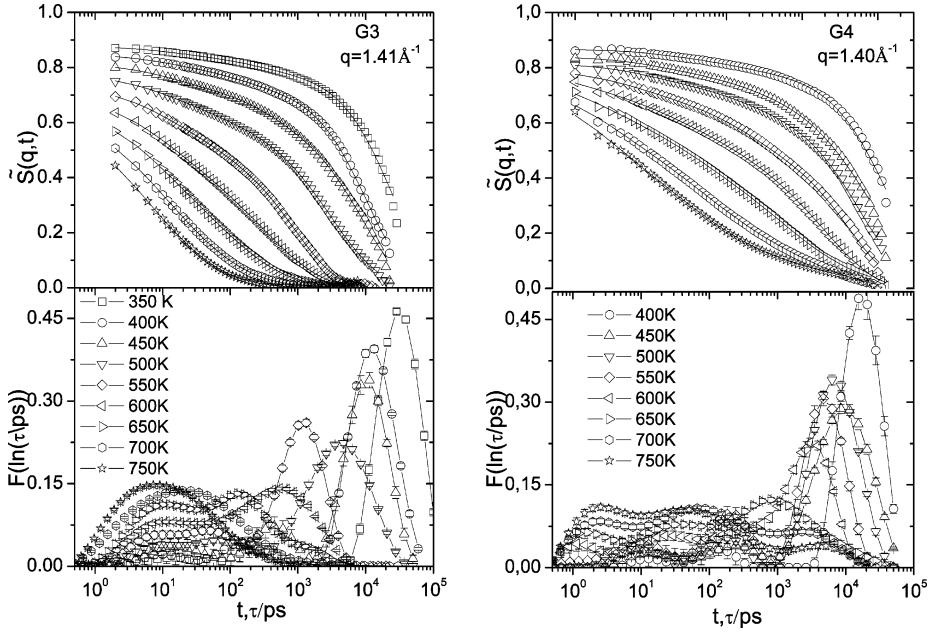

Figure 15. Temperature dependence of $\tilde{S}(q,t)$ correlation functions (upper panels) together with the corresponding DRTs (lower panels) for the two examined models.

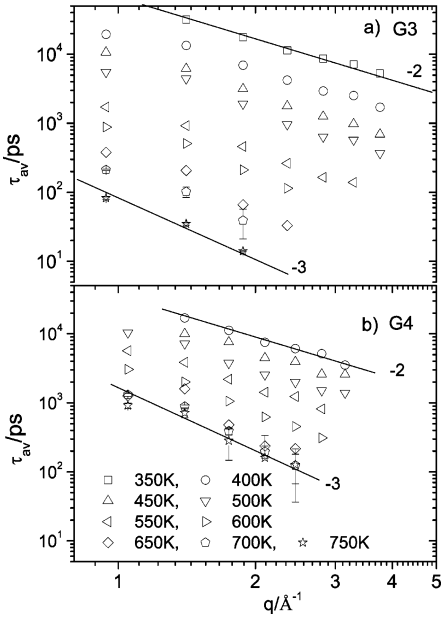

Figure 16. Average relaxation times of $\tilde{S}(q,t)$ for G3 (a) and G4 (b) models as a function of the magnitude of scattering vector for several temperatures. Error bars are comparable to the size of the symbols unless explicitly shown.

there is no further evidence that at these length scales such a mechanism could be involved. A similar high-q limiting behavior was observed in small X-ray scattering (SAXS) and neutron spin echo (NSE) experiments in poly(amidoamine) (PAMAM) dendrimer solutions. In one case,[79] authors argued that due to the rather small size of the dendrimers which exhibited this behavior (G = 3 and G = 4), their data bear resemblance to scattering from a polymer star (where a similar q dependence is found) and therefore could be accounted for, if a starlike structure with excluded volume effects was assumed. In another case,[17] although the authors noted that the q^{-2} scaling of the times is also detected at length scales shorter than the dendrimer dimensions, this behavior was considered to arise from longer length scale diffusional motion since it was argued that no contribution of internal relaxation processes to the decay of the dynamic structure factor could be detected. It should also be mentioned that a similar q^{-2} dependence of the α-relaxation process at the high-q limit in linear polymers was found[80] to be associated with the non-Gaussian behavior of the Van Hove self-correlation function $G(r,t)$ (that is, the non-Gaussian character of the scatterers' motion) at very short length scales. The present stage of analysis cannot be conclusive as to which of the above scenaria is more relevant to the observed behavior. Further investigation is left for a future study.

An explanation for the existence of two limiting slopes (q^{-2} at low and q^{-3} at high temperatures) may be in order, if we review the spectral behavior of the relative time distributions (Figure 11). Since the average time was calculated on the basis of the entire time window, contributions arising from the faster process are taken into account as well, affecting accordingly the overall average particularly at the high temperature regime. At lower temperatures the average time is practically determined by the behavior of the slower processes, which follows the q^{-2} scaling. In light of this observation, one can visually confirm that the change of slope regarding the q dependence takes place close to temperatures where the fast processes' amplitude begins to diminish.

C. Reorientational Motion. While dynamics described by $S(q,t)$ is relevant to scattering experiments, correlation functions probing local bond reorientation can be linked to nuclear magnetic resonance (NMR) measurements through the spectral density $J(\omega) = {}^1/_2\int_{-\infty}^{\infty} P_2(t)e^{i\omega t}\,dt$, where $P_2(t)$ is the second-order autocorrelation function

$$P_2(t) = \frac{1}{2}\langle 3[\hat{h}(t)\cdot\hat{h}(0)]^2 - 1\rangle \qquad (6)$$

$\hat{h}$ symbolizes the unit vector along an examined bond. For computational efficiency purposes, a representative behavior of local reorientational dynamics under the constraints imposed by the dendritic topology was

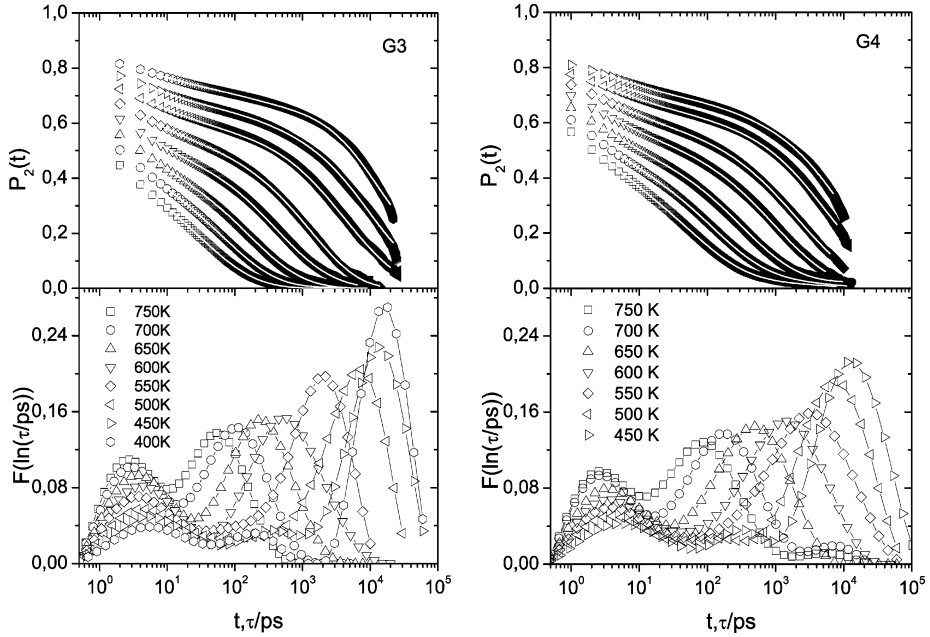

Figure 17. Upper panels: reorientational correlation functions for bonds belonging to the last generational shell. Lower panels: corresponding DRTs.

obtained by monitoring reorientation of the bonds belonging only to the last generational shell as this consists of more than half of the available bonds, while its beads can explore the entire dendrimer structure as a result of backfolding. To treat all dynamic data on a common basis, correlation functions were analyzed in terms of calculation of the DRTs as described in section V.B. $P_2(t)$ spectra (averaged over all relevant bonds and time origins) accompanied by the respective distributions are shown in Figure 17 for the two models examined at several temperatures. (Only correlation functions sufficiently relaxed within the available time windows were analyzed.)

The DRT spectra describing the reorientational correlation functions for the two models are much alike, bearing also similarity to the corresponding distributions resulted from the analysis of dynamic structure factor data (see Figure 15). At higher temperatures two dynamic processes can be discerned: a fast one showing a decreasing amplitude, but almost an unchanged characteristic time on temperature decrease, and a slower process with an increasing amplitude and relaxation time as temperature drops. For both models only at lower temperatures processes with intermediate time scales and relatively low amplitude are manifested. A distinct feature can be noticed when comparing spectra of the two models at the same temperature: distributions corresponding to the G4 model appear to be broader. This larger dispersion of the characteristic relaxation times is consistent with a higher level of dynamic heterogeneity.

On the basis of the general resemblance between $P_2(t)$ and $\tilde{S}(q,t)$ DRTs, one can resort to a similar assignment for the observed peaks. Actually, these two functions can probe similar dynamics provided that an appropriate selection of scattering vector is made. Namely, it is known that the time scale as well as the temperature dependence of α-relaxation in polymers, as probed by $P_2(t)$,[81] can be reproduced by dynamic structure factor data at a q value corresponding to the intermolecular peak of the static structure factor.[56,65] The closest analogue to that in the case of dendrimer

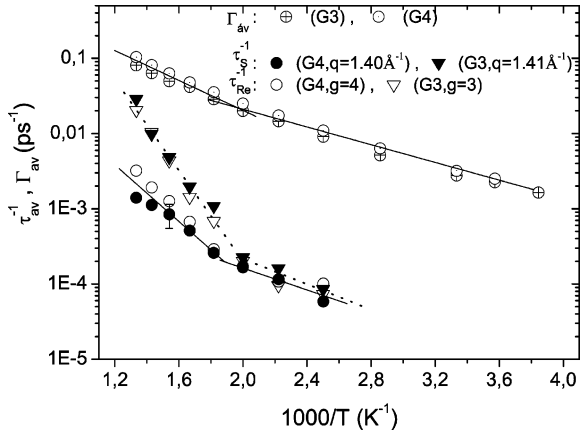

Figure 18. Average transition rates (Γ) for G3 (⊗) and G4 (⊙) systems. Inverse average relaxation times as probed by $P_2(t)$: G4 (○); G3 (▽). Corresponding solid symbols refer to inverse average times as probed by $\tilde{S}(q = 1.40$ Å^{-1}, $t)$ for G4 and $\tilde{S}(q = 1.41$ Å^{-1}, $t)$ for G3, respectively. Error bars are within the symbols' size unless explicitly shown.

melts as discussed in section IV.B is peak 3 of the dendrimer $S(q)$ (which arises from both intramolecular and intermolecular contributions) with a maximum position at $q \simeq 1.4$ Å^{-1}. In this context, similarity in correlation functions and respective DRTs between spectra displayed in Figures 15 and 17 are rather anticipated. A more quantitative comparison involving collation of the respective average relaxation rates appears in Figure 18. For a better overview of the dynamic behavior in local scale, average torsional transition rates presented earlier in Figure 14 are included as well. Evidently, average relaxation rates describing bond reorientational motion and dynamic structure factor data compare favorably not only in terms of absolute time scale but also in terms of temperature dependence, lending credence to the argument regarding their interconnection. For both models a characteristic change in the temperature dependence of relaxation rates takes place at a temperature close to the one indicated as a phenomenological glass transi-

tion according to static/structural and dynamic (transition rates) data. Although below that temperature relaxation rates describing the two dendrimer models are virtually indistinguishable, at higher temperatures G3 dynamics appears to be faster. In other words, at temperatures above the nominal T_g local relaxation is dendrimer size dependent. This observation is in line with the molecular size dependence of the segmental reorientation time in dendrimer solutions, as measured by relevant NMR experiments.[73,74] The same feature has also been noted in the freely jointed counterparts of the examined models[18] and was explained by means of an association of the slowest process observed in the pertinent DRTs, with the overall dendrimer motion. The same line of reasoning seems to offer a plausible explanation for the melt case as well.

A last issue that needs to be resolved is the significantly weaker temperature dependence and the considerably faster time scale manifested by the average transition rates compared to dynamics as probed by $P_2(t)$ and $\tilde{S}(q,t)$. The reasons for the elevated torsional rates are the relatively low-energy requirement for a jump to occur, together with the fact that both forward and consecutive backward jumps undergone by a dihedral angle are counted as successful transitions (as long as the minima of the neighboring potential well is crossed), contributing to the estimated average. On the other hand, such forward−backward pairs of jumps realized in very short time scales effectively leave the participating beads with no significant displacement relative to their initial positions, contributing thus to a minor degree to the relaxation of the dynamic structure factor or to the reorientation of the related bonds. A significant bead displacement or a bond reorientation would require higher energy, consorted with analogous cooperative motions of neighboring beads, which would render such motions much more temperature dependent compared to a simple dihedral jump, as is actually observed.

VI. Summary/Conclusions

Static and dynamic behavior of dendrimer molecules in the melt combines several features of polymeric and soft colloidal nature. A liquidlike ordering with a first neighbor shell close to $2R_g$ characterizes the amorphous melt state, which seems to lose a certain degree of its "homogeneity" as temperature lowers, in analogy to the observed development of spatial heterogeneities close to colloidal glass transition.[82] During the cooling process interpenetration between dendrimers increases, allowing the approach of dendrimer centers of mass and forming areas with distinct local density within the dendritic structure; it therefore plays a central role to alteration of the interdendrimer arrangement and to modification of intradendrimer local packing. A discontinuity in the temperature dependence of the specific volume accompanied by morphological differentiations in the dendrimer geometry signifies the onset of a glasslike transition. The synergy of both intramolecular and intermolecular factors in the manifestation of this transition is apparently reflected by the appearance and the associated temperature dependence of relevant diffraction peaks in the dendrimer static structure factor, particularly in the behavior of a maximum at the location of the intermolecular peak of a linear polymer's structure factor (q_{lin}^{inter}). The dynamic "signature" of this transition is expressed through a reduction of torsional mobility depending on the depth within the dendrimer structure and by a marked slowdown of the average local reorientational and translational (as expressed by the dynamic dendrimer structure factor at $q \simeq q_{lin}^{inter}$) motion. A more detailed comparison of local segmental motion between dendrimers with varying dendritic topology and linear polymers will be discussed in a future study.

The level of consistency of the above-described picture with pertinent experimental findings in several dendrimer systems as mentioned in the text leads us to believe that most of the phenomena observed capture features generic to the dendritic topology. On these grounds, such systems may serve as models for the exploration of soft-colloidal behavior in general, and more specifically near the glass transition, contributing to the elucidation of the underlying mechanisms and providing thus valuable information toward a molecularly engineered control of their physical properties.

Acknowledgment. Part of this work was carried out while the author was a visiting professor at Materials Science and Technology Department, University of Crete.

References and Notes

(1) Gao, C.; Yan, D. *Prog. Polym. Sci.* **2004**, *29*, 183−275.
(2) Yates, C.; Hayes, W. *Eur. Polym. J.* **2004**, *40*, 1257.
(3) Cloninger, M. J. *Curr. Opin. Chem. Biol.* **2002**, *6*, 742.
(4) Balogh, L.; Bielinska, A.; Eichman, J.; Valluzzi, R.; Lee, I.; Baker, J.; Lawrence, T.; Khan, M. *Chim. Oggi* **2002**, *20*, 35−40.
(5) Ballauff, M.; Likos, C. N. *Angew. Chem., Int. Ed.* **2004**, *43*, 2998−3020.
(6) Asteriadi, A.; Sigel, R.; Vlassopoulos, D.; Meier, G.; Dorgan, J.; Knauss, D. *Macromolecules* **2004**, *37*, 1016−1022.
(7) Harreis, H. M.; Likos, C. N.; Ballauff, M. *J. Chem. Phys.* **2003**, *118*, 1979−1988.
(8) Vlassopoulos, D.; Fytas, G.; Pakula, T.; Roovers, J. *J. Phys.: Condens. Matter* **2001**, *13*, R855−R876.
(9) Boas, U.; Heegaard, P. M. H. *Chem. Soc. Rev.* **2004**, *33*, 43.
(10) Parquette, J. *CR Chim.* **2003**, *6*, 779.
(11) Dykes, G. *J. Chem. Technol. Biotechnol.* **2001**, *76*, 903.
(12) Lyulin, S.; Darinskii, A.; Lyulin, A.; Michels, M. *Macromolecules* **2004**, *37*, 4676−4685.
(13) Li, Y.; Lin, S.; Goddard, W. *J. Am. Chem. Soc.* **2004**, *126*, 1872−1885.
(14) Furuta, P.; Frechét, J. *J. Am. Chem. Soc.* **2003**, *125*, 13173.
(15) Govorun, E.; Zeldovich, K.; Khokhlov, A. *Macromol. Theor. Simul.* **2003**, *12*, 705−713.
(16) Timoshenko, E.; Kuznetsov, Y.; Connolly, R. *J. Chem. Phys.* **2002**, *117*, 9050−9062.
(17) Rathgeber, S.; Monkenbusch, M.; Kreitschmann, M.; Urban, V.; Brulet, A. *J. Chem. Phys.* **2002**, *117*, 4047−4062.
(18) Karatasos, K.; Adolf, D. B.; Davies, G. R. *J. Chem. Phys.* **2001**, *115*, 5310−5318.
(19) Mark, S.; Sandhyarani, N.; Zhu, C.; Campagnolo, C.; Batt, C. *Langmuir* **2004**, *20*, 6808.
(20) Li, X.; Curry, M.; Wei, G.; Zhang, J.; Barnard, J.; Street, S.; Weaver, M. *Surf. Coat. Technol.* **2004**, *177−178*, 504.
(21) Knoll, W.; Han, M.-Y.; Li, X.; Hernandez-Lopez, J.-L.; Manna, A.; Mullen, K.; Nakamura, F.; Niu, L.; Robelek, R.; Schmid, E. L.; Tamada, K.; Zhong, X. *J. Nonlinear Opt. Phys.* **2004**, *13*, 229.
(22) Johnson, R. C. *Electron. Eng. Times* **2004**, 16.
(23) Herr, D.; Zhirnov, V. *Solid State Technol.* **2004**, *47*, 26.
(24) Caminade, A.; Majoral, J. *Acc. Chem. Res.* **2004**, *37*, 341.
(25) Balzani, V.; Ceroni, P.; Maestri, M.; Vicinelli, V. *Curr. Opin. Chem. Biol.* **2003**, *7*, 657.
(26) Dorgan, J.; Knauss, D.; Al-Muallem, H.; Huang, T.; Vlassopoulos, D. *Macromolecules* **2003**, *36*, 380.
(27) Ozerin, A.; Muzafarov, A.; Gordeliy, V.; Kuklin, A.; Ignateva, G.; Krykin, M.; Ozerina, L.; Shumilkina, N.; Islamov, A. K.; Sharipov, E. Y.; Mukhamedzyanov, R. *Macromol. Symp.* **2003**, *195*, 171−178.

(28) Dantras, E.; Caminade, A.; Majoral, J.; Lacabanne, C. *J. Phys. D: Appl. Phys.* **2002**, *35*, 5−8.
(29) Kruger, J. K.; Veith, M.; Elsasser, R.; Manglkammer, W.; Le Coutre, A.; Baller, J.; Henkel, M. *Ferroelectrics* **2001**, *259*, 27−36.
(30) Hay, G.; Mackay, M. E.; Hawker, C. J. *J. Polym. Sci., Polym. Phys.* **2001**, *39*, 1766−1777.
(31) Rogunova, M.; Lynch, T.; Pretzer, W.; Kulzick, M.; Hiltner, A.; Baer, E. *J. Appl. Polym. Sci.* **2000**, *77*, 1207.
(32) Huwe, A.; Appelhans, D.; Prigann, J.; Voit, B.; Kremer, F. *Macromolecules* **2000**, *33*, 3762.
(33) Hawker, C.; Farrington, P.; Mackay, M.; Wooley, K.; Frechét, J. *J. Am. Chem. Soc.* **1995**, *117*, 4409.
(34) Liu, H.; Wilen, C. *J. Polym. Sci., Polym. Phys.* **2004**, *42*, 1235−1242.
(35) Zacharopoulos, N.; Economou, L. *Macromolecules* **2002**, *35*, 1814−1821.
(36) Stutz, H. *J. Polym. Sci., Polym. Phys.* **1995**, *33*, 333−340.
(37) Wooley, K.; Hawker, C.; Pochan, J.; Frechét, J. *Macromolecules* **1993**, *26*, 1514−1519.
(38) Yoshimoto, K.; Jain, T.; Workum, K.; Nealey, P.; de Pablo, J. *Phys. Rev. Lett.* **2004**, *93*, Art. 175501.
(39) Chong, S.; Fuchs, M. *Phys. Rev. Lett.* **2002**, *88*, Art. 185702.
(40) Richter, D.; Monkenbusch, M.; Willner, L.; Wischnewski, A.; Arbe, A.; Colmenero, J. *Polym. Int.* **2002**, *51*, 1211−1218.
(41) Cates, M. *Annales Henri Poincare* **2003**, *4*, S647−S661.
(42) Pham, K.; Puertas, A.; Bergenholtz, J.; Egelhaaf, S.; Moussaid, A.; Pusey, P.; Schofield, A.; Cates, M.; Fuchs, M.; Poon, W. *Science* **2002**, *296*, 104−106.
(43) Weeks, E.; Weitz, D. *Phys. Rev. Lett.* **2002**, *89*, Art. 095704.
(44) Tata, B.; Mohanty, P.; Valsakumar, M. *Phys. Rev. Lett.* **2002**, *8801*, Art. 018302.
(45) Mayo, S.; Olafson, B.; Goddard, W., III *J. Phys. Chem.* **1990**, *94*, 8897.
(46) Mazo, M.; Zhilin, P.; Gusarova, E.; Sheiko, S.; Balabaev, N. *J. Mol. Liq.* **1999**, *82*, 105−116.
(47) Cagin, T.; Wang, G. F.; Martin, R.; Breen, N.; Goddard, W. A. *Nanotechnology* **2000**, *11*, 77−84.
(48) Cagin, T.; Wang, G.; Martin, R.; Zamanakos, G.; Vaidehi, N.; Mainz, D.; Goddard, W. *Comput. Theor. Polym. Sci.* **2001**, *11*, 345−356.
(49) Lyulin, A. V.; Davies, G. R.; Adolf, D. B. *Macromolecules* **2000**, *33*, 3294−3304.
(50) Nosé, S. *J. Chem. Phys.* **1984**, *81*, 511.
(51) Melchionna, S.; Ciccoti, G.; Holian, B. *Mol. Phys.* **1993**, *78*, 533.
(52) Forester, T.; Smith, W. CCLRC, Daresbury Laboratory, Daresbury, Warrington Wa4 4AD, England. DL_POLY is a parallel molecular dynamics package developed at Daresbury laboratory and is a property of the Council for the Central Laboratory of the Research Councils (CCLRC).
(53) Naylor, A.; Goddard, W. *J. Am. Chem. Soc.* **1989**, *111*, 2339.
(54) Cavallo, L.; Fraternali, F. *Chem.—Eur. J.* **1998**, *4*, 927−934.
(55) McKenna, G. *Comprehensive Polymer Science*; Pergamon: Oxford, 1989; Vol. 2.
(56) Paul, W.; Smith, G. *Rep. Prog. Phys.* **2004**, *67*, 1117.
(57) Wooley, K.; Klug, C.; Tasaki, K.; Schaefer, J. *J. Am. Chem. Soc.* **1997**, *119*, 53.
(58) Gorman, C.; Hagger, M.; Parkhurst, B.; Smith, J. *Macromolecules* **1998**, *31*, 815.
(59) Ozerin, A. *Macromol. Symp.* **2001**, *174*, 93−102.
(60) Allen, M.; Tildesley, D. *Computer Simulation of Liquids*; Oxford Science Publications: New York, 1997.
(61) Higgins, J.; Benoit, H. *Polymers and Neutron Scattering*; Clarendon Press: Oxford, 1994.
(62) Boris, D.; Rubinstein, M. *Macromolecules* **1996**, *29*, 7251−7260.
(63) Scherrenberg, R.; Coussens, B.; van Vliet, P.; Edouard, G.; Brackman, J.; deBrabander, E.; Mortensen, K. *Macromolecules* **1998**, *31*, 456−461.
(64) Honnell, K.; McCoy, J.; Curro, J.; Schweizer, K.; Narten, A.; Habenschuss, A. *J. Chem. Phys.* **1991**, *94*, 4659.
(65) Richter, D.; Monkenbusch, M.; Arbe, A.; Colmenero, J. *J. Non-Cryst. Solids* **2001**, *287*, 286.
(66) The maxima locations of peak 3 as a function of temperature for both inter- and total-$S(q)$ exhibit a linear dependence with no evidence of change of slope in the examined temperature range.
(67) Guinier, A. *X-ray Diffraction;* Freeman & Co.: San Francisco, 1963.
(68) Vlassopoulos, D.; Pakula, T.; Fytas, G.; Roovers, J.; Karatasos, K.; Hadjichristidis, N. *Europhys. Lett.* **1997**, *39*, 617.
(69) Pakula, T.; Vlassopoulos, D.; Fytas, G.; Roovers, J. *Macromolecules* **1998**, *31*, 8931.
(70) Götze, I.; Harreis, H.; Likos, C. *J. Chem. Phys.* **2004**, *120*, 7761−7771.
(71) Gorman, C.; Smith, J. *Polymer* **2000**, *41*, 675.
(72) Mazo, M.; Shamaev, M.; Balabaev, N.; Darinskii, A.; Neelov, I. *Phys. Chem. Chem. Phys.* **2004**, *6*, 1285−1289.
(73) Meltzer, A.; Tirrell, D.; Jones, A.; Inglefield, P.; Hedstrand, D.; Tomalia, D. *Macromolecules* **1992**, *25*, 4541−4548.
(74) Meltzer, A.; Tirrell, D.; Jones, A.; Inglefield, P. *Macromolecules* **1992**, *25*, 4549−4552.
(75) Murat, M.; Grest, G. *Macromolecules* **1996**, *29*, 1278−1285.
(76) Provencher, S. A general-purpose constrained regularization method for inverting photon correlation data. In *Photon Correlation Techniques in Fluid Mechanics*; Schulz-DuBois, E. O., Ed.; Springer-Verlag: Berlin, 1983.
(77) Moe, N.; Ediger, M. *Macromolecules* **1995**, *28*, 2329−2338.
(78) Karatasos, K.; Ryckaert, J. *Macromolecules* **2001**, *34*, 7232−7235.
(79) Prosa, T.; Bauer, B.; Amis, E. *Macromolecules* **2001**, *34*, 4897−4906.
(80) Colmenero, J.; Alvarez, F.; Arbe, A. *Phys. Rev. E* **2002**, *65*, Art. 041804.
(81) Dejean de la Batie, R.; Lauprêtre, F.; Monnerie, L. *Macromolecules* **1989**, *22*, 2617−2622.
(82) Tokuyama, M.; Teradab, Y.; Oppenheim, I. *Physica A* **2002**, *307*, 27.

MA050155X